S.I. Jackson.
"Scaled Cylinder Test Experiments with Insensitive PBX 9502 Explosive."
In Proceedings of the 15th International Detonation Symposium, Office of Naval Research, pp. 171-180 (Office of Naval Research, 2015)

Scaled Cylinder Test Experiments with Insensitive PBX 9502 Explosive

Scott I. Jackson
Shock and Detonation Physics Group
Weapons Experiments Division
Los Alamos National Laboratory
Los Alamos, New Mexico, USA

Abstract. Five copper cylinder tests were performed with the insensitive explosive formulation PBX 9502. The tests spanned a range of sizes corresponding to scales of 0.25, 0.50, and 2.00 relative to the conventional 25.4-mm-inner-diameter test. This scale variation allows evaluation of effect of charge scale on the energy release in insensitive explosives, which have longer reaction zone lengths than conventional high explosives. Wall velocity histories allow measurement of the work available from the detonation products and ultimately support product equation-of-state development. We report the raw wall velocity history records, fit analytical forms to this data, and calculate the Gurney and kinetic-energy history associated with the cylinder wall during expansion.

Introduction

The detonation cylinder test is a standard high explosive performance diagnostic used to derive detonation product equation-of-state information[1,2]. Studies commonly use the velocity versus time history of the metal wall to quantify an explosive's product state capability to accelerate metal[3]. The cylinder test is also used to derive fit parameters for equation-of-state models[4].

We present the results of recently performed cylinder tests with the insensitive explosive formulation PBX 9502, composed of 95% TATB explosive and 5% Kel-F 800 (Polychlorotrifluoroethylene) binder polymer. Our cylinders were 0.25-, 0.50-, and 2.00-scaled designs of the conventional 25.4-mm inner-diameter test geometry[2]. This scaling was introduced to determine its effect on the energy release associated with the multi-scale reaction zone length of PBX 9502, which is thought to exhibit fast and slow reaction length scales of 0.2 mm and 1.5 mm, respectively. Several aspects of the wall velocity histories are presented and analyzed, including: early wall ringing associated with the initial shock breakout, the subsequent smooth wall acceleration, and the terminal velocity. The results are compared to previous tests and the effect of scale is discussed. Gurney and kinetic-energy histories will also be reported. A separate work details the product equation of state derivation from these results[5].

Experimental Details

The experimental geometry consisted a copper tube supported by a Delrin and aluminum assem-

Approved for unlimited release: LA-UR-14-24823

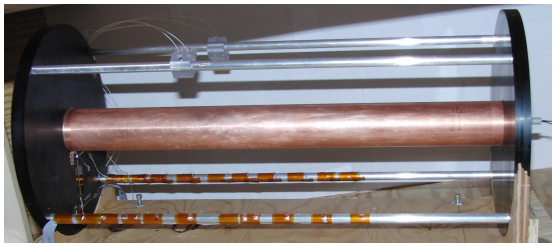

Fig. 1. The cylinder test geometry.

Table 1. Scaled cylinder test dimensions. Measurement tolerance was 50 μm. Standard test (25 mm ID) dimensions included in italics for reference.

Scale Factor	Length (mm)	ID (mm)	OD (mm)	t (mm)
0.25	76.20	6.36	7.62	0.63
0.50	152.4	12.70	15.24	1.27
1.00	*304.80*	*25.40*	*30.48*	*2.54*
2.00	609.60	50.80	60.96	5.08

bly as shown in Fig. 1. Cylinder tests are commonly performed with a standardized and scalable range of dimensions that fixes the ratio of the copper wall area to that of the explosive area across the tube cross section as detailed in Table 1. In this geometry, that ratio is 0.440. Under this constraint, any scaled variant is expected to yield identical wall velocity versus time data when the time axis is normalized by the test scale *assuming that the explosive energy yield is invariant of scale.*

When scale effects are not being measured, most tests are predominately fielded at the 1.00 scale to facilitate comparison with historic data. That said, the larger reaction zones and failure diameters associated with non-ideal explosive may necessitate larger scales. Conversely, some researchers often field smaller scales to accommodate limited budgets or explosive load limits at test sites.

Each test utilized time-of-arrival pins to measure the detonation velocity, four PDV probes to measure the cylinder wall motion, a streak camera for front shape measurement (not discussed in the present manuscript), and a framing camera for images of the cylinder wall expansion.

Copper Pedigree

All cylinder tests dimensions were scaled from the 1-in standard test [1–3] as detailed in Table 1. The copper grade was C101 Oxygen-free copper with a dead soft temper. Metallurgical analysis verified the annealed state after machining (8-20 Rockwell F hardness) and measured grain sizes on the order of 50 μm. Use of annealed copper is standard cylinder-test practice to prevent premature wall rupture during expansion. Grain size analysis ensured that the cylinder wall thickness t was composed of a sufficient number of grains (at least 10) so that fracture along single grain boundary would not necessarily result in a macroscopic wall rupture.

Explosive Fill

The copper cylinders were filled with right-circular cylinders of PBX 9502 explosive. PBX 9502 is an insensitive munition developed by the US Department of Energy and is composed of 95% TATB explosive and 5% Kel-F 800 polymer binder. PBX 9502 material used in this test series was cored from a 254-mm-diameter $\times$ 54-mm-long hydrostatically pressed billet of lot HOL88H891-008 prills.

It was necessary to machine the flexible PBX 9502 cores in multiple segments in order to achieve good dimensional tolerances. Thus, the explosive fill for each test was composed of a number of pieces as given in Tab. 2. Finished dimensions and densities (measured via immersion densitometry) for each segment are listed in Tables 3–5. Pieces were located in each cylinder such that density increased in the direction of detonation propagation with the lowest density segments adjacent to the booster charge as indicated in the tables.

Table 2. Explosive cylinder dimensions per test.

Test Scale	Cylinders per Test	Cylinder L/D
0.25	2	6.0
0.50	3	4.0
2.0	12	1.0

Due to machining tolerances, annular voids on the order of 20, 10, and 50 μm were present be-

Table 3. 0.25-scale cylinder PBX 9502 densities. Each part was 6.32 $\pm$ 0.01 mm in diameter and 38.10 $\pm$ 0.01 mm in length.

Test	Part	Density (g/cc)	Test	Part	Density (g/cc)
1	1	1.892	2	1	1.895
1	2	1.893	2	2	1.896

Table 4. 0.50-scale cylinder PBX 9502 densities. Each part was 12.69 $\pm$ 0.01 mm in diameter and 50.85 $\pm$ 0.01 mm in length.

Test	Part	Density (g/cc)	Test	Part	Density (g/cc)
1	1	1.886	2	1	1.887
1	2	1.888	2	2	1.888
1	3	1.888	2	3	1.888

tween the copper ID and explosive OD for the 0.25, 0.50, and 2.00-scale tests respectively. These voids were filled with Dow Corning Sylgard 184 Silicone Elastomer to adhere the assembly together and also to prevent product jetting ahead of the detonation. For the larger-aspect-ratio 0.25-scale HE cylinders, each pellet typically exhibited an interference fit at one end and a free-running fit at the other due to flexing during lathe machining. The smaller aspect ratio explosive cylinders in the 0.50- and 2.00-scale tests were much more uniform in their outer diameter and fit quality.

Each test was boosted with an HMX-based (PBX 9501) cylindrical pellet that was of comparable diameter to the explosive fill and with an aspect ratio of unity. The 0.25-scale tests were initiated with Teledyne RISI RP-2 detonators, while the larger tests were initiated with RP-1 detonators. The booster and initiators were located outside of the copper cylinder.

Detonation Time-of-Arrival Diagnostic

The propagation of the detonation front along the axial length of each cylinder was measured using 22 equally spaced shorting wires. No wires were placed within a length of two charge diameters of the booster in order to allow the overdriven wave to relax to a steady velocity. Each wire consisted of a

Table 5. 2.00-scale cylinder PBX 9502 densities. Each part was 50.75 $\pm$ 0.01 mm in diameter and 50.80 $\pm$ 0.01 mm in length.

Test	Part	Density (g/cc)	Test	Part	Density (g/cc)
1	1	1.884	1	7	1.887
1	2	1.884	1	8	1.887
1	3	1.885	1	9	1.887
1	4	1.886	1	10	1.888
1	5	1.887	1	11	1.889
1	6	1.887	1	12	1.889

50.8 μm-diameter (44 AWG) shielded copper magnet wire that was located on the outer cylinder diameter. The wires were raised to an electrical potential of 75.0 V through use of an RC circuit, with the copper tube acting as ground. Arrival of the shock associated with the detonation wave at each wire drove the cylinder wall through the wire shielding and allowed current to flow from the high-voltage wire to ground, resulting in a measured voltage drop across the resistor in the RC circuit. Probes locations were measured to within 30 μm and the pin voltage was sampled with a bandwidth of 1 GHz (5 GS/s digitizer rate) during each test.

Wall Motion Diagnostic

Photon Doppler Velocimetry (PDV), a heterodyne interferometry technique, was used to measure the wall motion during each experiment. Four collimated PDV probes with a 20-100 mm working distance and a with a spot size of less than 350 μm. The probes were spaced around the cylinder (approximately 40° radially apart) and aligned to measure the cylinder wall motion at a distance that was 1/3 of the total cylinder length from the breakout end. Two of the probes were located normal to the cylinder wall and the remaining two were located normal to the estimated 7° cylinder wall angle occurring after detonation passage. Each surface was sanded with 200-grit sandpaper and inspected for diffuse reflectivity. For the 0.25 and 0.50-scale tests, probes were spaced 50 mm away from the cylinder wall. For the 2.00-scale tests, probes were located 100 mm from the wall. Additionally, each assembly was designed to ensure that nothing would interfere with the wall

motion prior to impact of the cylinder wall onto the probe. PDV data was recorded at a bandwidth of 20 GHz (50 GS/s digitizer rate) and reduced using a 32-bit Fourier window size and a 4096-bit window step size.

Experimental Results

Measured Detonation Velocity

Detonation velocities were calculated from the time-of-arrival diagnostic data by assuming a steady axial wave velocity along the length of the charge. Probes distances and trigger times were fit to x and t respectively in

$$x = D\,t + t_0 \tag{1}$$

A least-squares fit was used to optimize the detonation velocity D and apparent initiation time t_0. The fitted velocity results and standard error (listed as uncertainty) are given in Tab. 6 for each test. Both detonation velocities and standard error decreased with charge diameter. Test 025-1 was found to have the highest standard error (0.63% of D). For all other tests, the standard error was below 0.12% of D.

Table 6. Measured detonation phase velocities at the copper wall.

Test Name	ID (mm)	D (mm/μs)	$\pm$ Std. Error (mm/μs)
025-1	6.36	7.292	0.046
025-2	6.36	7.334	0.009
050-1	12.70	7.494	0.004
050-2	12.70	7.489	0.004
200-1	50.80	7.653	0.003

The observed diameter effect is shown in Fig. 2 as a function of the inverse charge radius for the present data and previously published PBX 9502 cylinder test data from Refs. 2, 3, and 6. Also shown is a diameter effect curve for unconfined PBX 9502 rate sticks from the Detonation Shock Dynamics mode for a PBX 9502 calibration[7] and a single data point for an unconfined 8.5-mm-diameter PBX 9502 rate stick performed by the author.

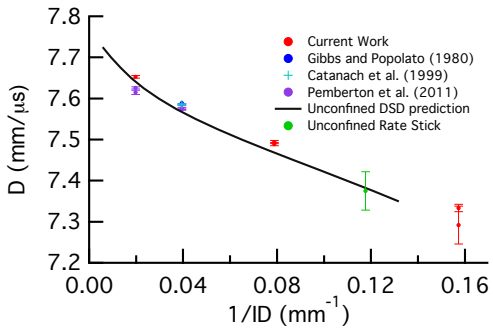

Fig. 2. Diameter effect data for unconfined and copper confined PBX 9502 charges. Detonation velocities are not adjusted for density effects.

The present scaled cylinder test velocity data agree well with the prior cylinder test work of Refs. 2 and 3. The data also lie above the unconfined numerical prediction. This trend is consistent with the understanding that the presence of the metal confinement reduces the transverse flow expansion in the reaction zone, allowing more of the combustion energy to drive the detonation shock. One of the 0.25-scale tests (025-1) does not follow this trend and lies on the extrapolated DSD curve, indicating that there was insufficient confinement between the copper and the explosive. However, the remaining 0.25-scale test (025-2) lies above the unconfined trend. Gaps on the order of the detonation reaction zone length (100 μm for PBX 9502) would result in unconfined detonation velocities.

A single 1.0-scale cylinder test and both 2.0-scale cylinder tests of Ref. 6 are also seen to lie below the confined diameter effect trend. Surprisingly, the 2.0-scale data from Ref. 6 lies below the diameter-effect curve prediction for unconfined charges. These deviations from the trend may be due to use of low-density charges or the presence of an air-gap between the explosive and copper cylinder wall.

Framing Imaging Data

Framing images of the expanding cylinder in test 200-1 and 050-2 are shown in Figs. 3 and 4.

After transit of the detonation, the cylinder wall is accelerated radially outwards by the high pressure combustion products. Initially, the wall experi-

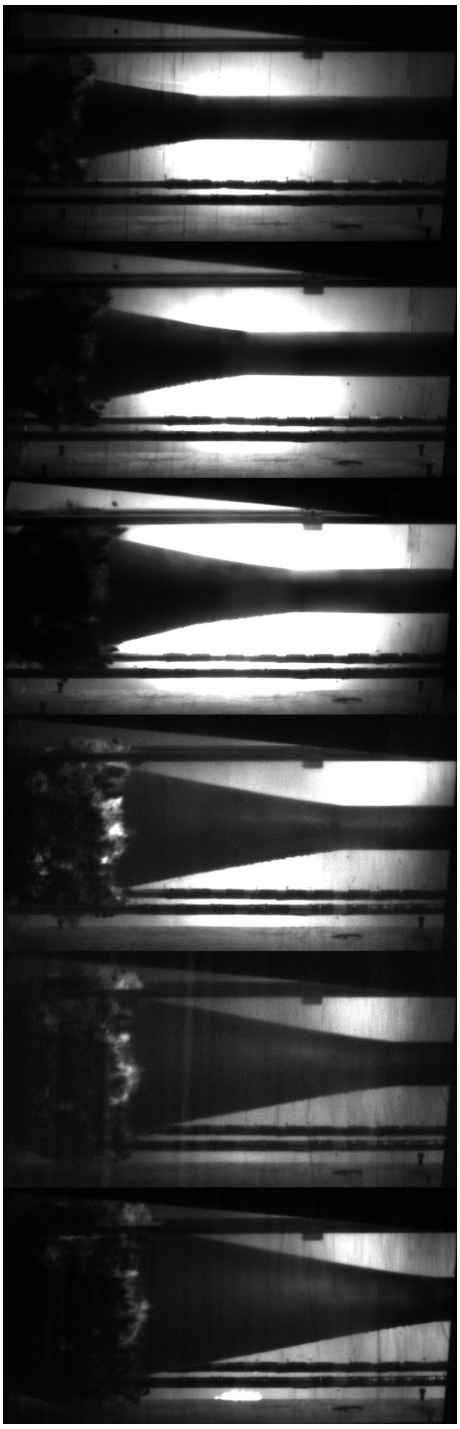

Fig. 3. Framing images of test 200-1 taken 8.75 μs apart.

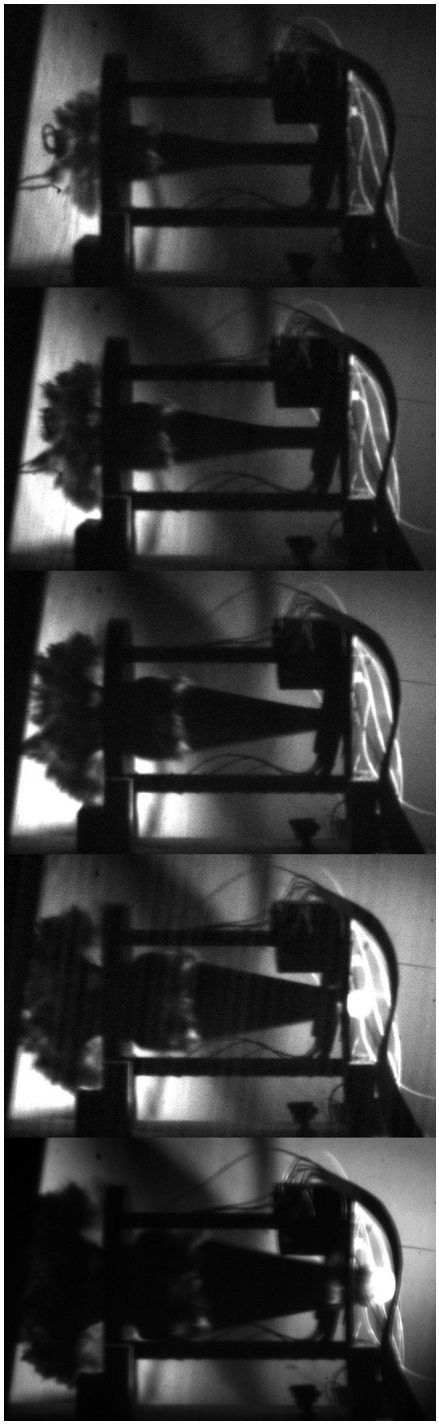

Fig. 4. Framing images of test 050-2 taken 3.75 μs apart.

ences a rapid acceleration phase and has a concave-outwards profile. After a duration of several microseconds (specific values depend on the product equilibrium time and cylinder wall thickness), corresponding to 10–20 mm of axial length in the framing image, wall acceleration decreases significantly and approaches a steady-state velocity value V_∞. At this point, the wall assumes a straight profile that is angled away from the initial tube axis. With the assumption that the velocity vector of wall motion is predominately radially outwards, the instantaneous wall angle θ_w relative to the tube axis can be approximated by

$$\theta_w(t) \approx \arctan\left(\int \frac{V_r(t)}{D(t)} dt\right) \tag{2}$$

where V_r is the radial component of the wall velocity and D is the detonation velocity. In reality, the deforming wall also develops a small component of motion in the axial upstream direction which is quantified in a separate work[5]. However, near the end of the acceleration process, the cylinder wall angle will approach

$$\theta_{w,\infty} \rightarrow \arctan\left(\frac{V_\infty}{D}\right) \tag{3}$$

by assuming a steady detonation velocity and neglecting the initial velocity transient. For the range of wall and detonation velocities measured in the present experiments, $\theta_{w,\infty}$ ranges from 10.8°–11.1°. Wall velocity profiles are reported below.

Measured wall velocities

Examples of the wall motion measured by the PDV probes are shown in velocity-time spectrograms in Figs. 5–7. The PDV profiles provide increased resolution relative to the framing camera data. All probe profiles exhibit characteristically similar features. The detonation is supersonic relative to the sound speed of the copper tube and drives a shock wave into the wall. Upon initial shock breakout, the outer wall diameter discontinuously accelerates the wall to approximately 0.9 mm/μs. The wall velocity then accelerates in an oscillatory fashion ("rings-up") for several microseconds as a series of shocks and expansion fans equilibrate the pressure across the inner and outer wall surfaces. The amplitude of the ringing oscillations decreases

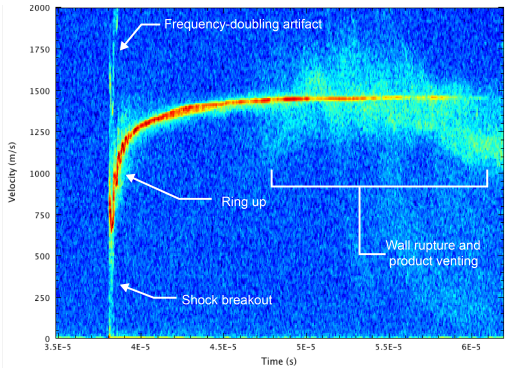

Fig. 5. Velocity spectrogram for PDV4 from 025-2.

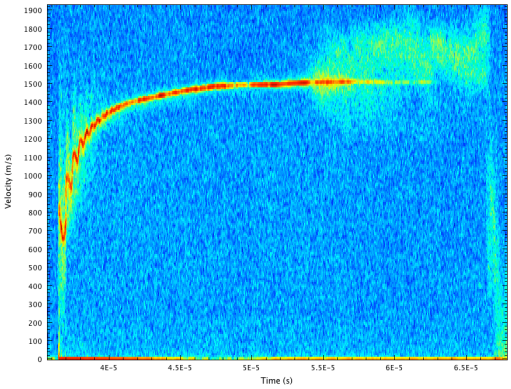

Fig. 6. Velocity spectrogram for PDV1 from 050-2.

over time as the cylinder expansion decreases the product gas pressure. Eventually, the product gas pressure no longer exerts significant force on the cylinder and the wall velocity approaches a constant value of V_∞. For the present experiments, V_∞ is approximately 1.5 mm/μs.

At some point in the cylinder expansion process, the wall stretches and thins sufficiently that it fails. This rupture allows detonation products gases inside the cylinder to expand ahead of the wall. These products can also carry fragments of the tube wall in the product jet. On the PDV spectrograms, this feature appears as a diffuse spray of energy covering a wide ($>$ 0.3 mm/μs) velocity range. The higher velocities indicate product expansion on the probe measurement axis, while lower velocities may indicate slower moving material or expansion significantly off of the measurement axis. Premature wall failure and product venting will affect the wall ve-

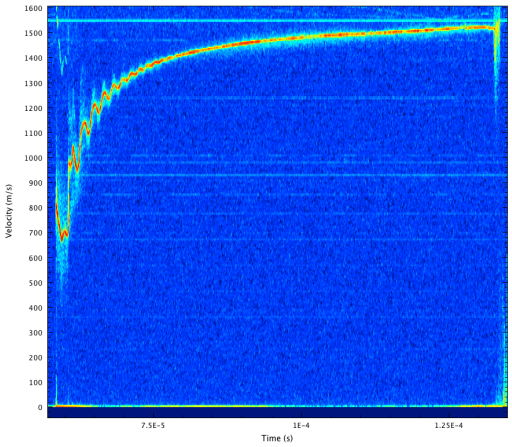

Fig. 7. Velocity spectrogram for PDV3 from 200-1.

locity trajectory, resulting in lower values of V_∞. For this reason, most acceleration stops when product jetting appears (*cf.* Fig. 5 after 48 μs and Fig. 6 after 54 μs).

Analysis

Wall Motion

During cylinder test analysis, the wall motion is typically fit to an analytic function. This technique simplifies presentation and comparison with numerical results. Traditionally[4,8], the following empirical fitting form has been used to match the measured velocity–time relationship for the tube wall

$$R\left(t\right) - R_0 = \frac{V_\infty \left(t - t_0\right) f\left(t\right)}{\frac{2V_\infty}{a_0} f\left(0\right) + f\left(t\right)} \tag{4}$$

with

$$f\left(t\right) = \left(1 + t - t_0\right)^\omega - 1 \tag{5}$$

where t_0 is a temporal shift parameter to accommodate delayed first motion.

As described in Ref. 4, this fitting form was designed around several constraints, including: (1) zero initial wall velocity $dR/dt(t_0) = 0$; (2) an asymptotic approach to a steady wall velocity V_∞ at long times $dR/dt(\infty) \rightarrow V_\infty$; (3) an initial finite acceleration term $d^2R/dt^2(t_0) = a_0$ associated with a finite product pressure loading; (4) a negative initial isentrope slope, implying $d^3R/dt^3(t_0) < 0$; and (5) monotically decreasing pressure for all time $d^5R/dt^5(t) > 0$. The fit does not capture the initial, compressible ring-up behavior present when the tube wall is driven supersonically. Instead, it smoothly averages through this acceleration regime.

Historically[2], radial cylinder wall motion was recorded using a streak camera with the streak slit located perpendicular to the long axis of the tube and backlighting from a bright light source, such as an Argon flash[9]. Data derived from this diagnostic was directly fit to Eq. 4. Modern interferometry techniques such as PDV, VISAR, and Fabry-Perot can be analyzed to yield the wall velocity–time relationship directly. Data from these diagnostics can be integrated in time and fit to Eq. 4. Alternatively, Eq. 4 can be differentiated in time to obtain a fitting form that is a function of $V_r(t)$, as is done in the present manuscript.

Direct measurement of $V_r(t)$ is appealing for experiments with the ultimate goal of determining the detonation-product pressure driving the wall, as it only requires differentiating the $V_r(t)$ data or fit a single time (rather than the two derivatives necessary when $X_r(t)$ is measured). Additionally, probe-based interferometry techniques more easily allow for multiple probes to be spaced a different axial and radial locations along the tube wall. Use of several probes minimizes the chance of data loss due to premature wall failure. Premature wall failure can occur due to poorly prepared copper or the presence of product-gas jetting. Such jetting commonly occurs when large air gaps exist in (i) explosives with significant porosity, (ii) near poorly mated explosive pellet joints, or (iii) near poorly mated explosive-copper joints.

Figure 8 illustrates the fit quality typical of Eq. 4. In the top part of Fig. 8, analytic fit curves (dashed black curves) from Eq. 4 with parameters given in Tab. 7 are plotted over the experimental PDV datapoints for the data from Figs. 5–7. The curves are shown to approximate the average wall motion well, but do not capture the ringing features associated with the compressibility effects present in the wall for early times.

The bottom part of Fig. 8 indicates the "fit residual" for each trace as a percentage of the wall velocity. Fit residuals were calculated by taking the absolute difference between the fit and each experimental datapoint, normalized by the experimental

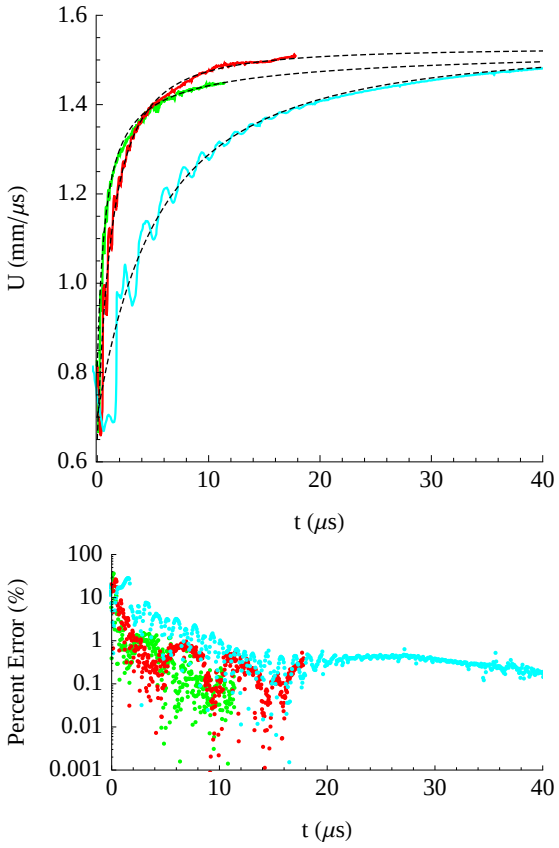

Fig. 8. Comparison of analytic fit to experimental data from Figs. 5–7. Green = 0.25 scale; red = 0.50 scale, and cyan = 2.00 scale. (Top) Velocity versus time. (Bottom) Percent error between experiment and fit.

value. As the ringing amplitude decays, the residual errors decrease to between 0.1–1%. When ringing is significant, the residual errors are as large as 10%. Thus, the analytic fits do not provide a good approximation of the wall motion during the compressible acceleration phase. It is worth noting that when wall motion is subsonic, no ringing is present. Such motion exists when the confiner sound speed exceeds the detonation velocity as shown for ANFO explosive in Refs. 10 and 11.

Fitting parameters obtained from fitting the velocity-time data to the temporal derivative of Eq. 4 are tabulated in Table 7.

Table 7. Wall motion fits to measured $V_r(t)$.

Test	PDV	θ_p	V_∞	a_0	ω	t_0
025-1	1	0°	1.447	2.517	0.969	38.4
025-1	2	7°	1.800	4.299	2.1×10^{-8}	37.8
025-1	3	0°	1.587	3.107	0.516	38.5
025-1	4	7°	1.403	1.684	1.369	37.5
025-2	1	0°	N/A	N/A	N/A	N/A
025-2	2	7°	1.433	2.420	1.078	37.6
025-2	3	0°	1.557	3.179	0.495	38.7
025-2	4	7°	1.549	3.656	0.495	37.8
050-1	1	0°	1.562	1.807	0.833	36.1
050-1	2	7°	1.450	1.113	1.256	34.9
050-1	3	0°	1.521	1.562	0.943	35.9
050-1	4	7°	1.541	1.709	0.852	34.7
050-2	1	0°	1.529	1.544	0.940	35.9
050-2	2	7°	1.603	1.664	0.793	35.2
050-2	3	0°	1.464	1.084	1.276	35.6
050-2	4	7°	1.550	1.454	0.983	34.9
200-1	1	0°	1.518	0.401	0.961	59.9
200-1	2	7°	1.516	0.377	0.984	55.3
200-1	3	0°	1.539	0.419	0.941	56.3
200-1	4	7°	1.495	0.322	1.060	59.3

Scaling

As discussed, all tests in the series contained a fixed ratio of explosive fill volume to confiner volume. Under this design, explosive that are scale-invariant (release a constant energy per unit volume with a reaction completion time that is very small relative to the wall acceleration time, regardless of the charge size) should accelerate all the confiner material to a similar terminal velocity, regardless of the test scale. Additionally, under this assumption, all velocity profiles should also overlay when the timebase is normalized by the scale factor (SF) associated with each test[1,12].

Figure 9 tests this assumption by plotting wall velocity versus scaled time. The two larger (0.50 and 2.00) scale traces overlay well to within 0.5% over the full test time, indicating equivalent energy release at each scale. However, the smallest (0.25) scale indicates a significant (6%) velocity deficit in the late time motion relative to the 2.00 scale test. Examination of the early time motion in the inset of Fig. 9 shows that at extremely early (scaled) times,

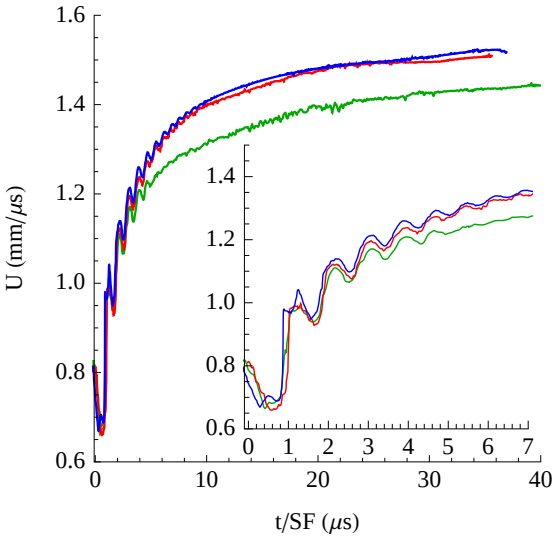

Fig. 9. Scaled traces from Figs. 5–7. Green = 0.25 scale; red = 0.50 scale, and blue = 2.00 scale.

from 0–2 scaled μs, there is negligible different between each scale. After 2 μs, however, the 0.25 scale trace increasingly drops below the 2.00 scale trace until 10 μs, where the velocity deficit remains approximately constant thereafter.

This effect is quantified in Fig. 10, which shows

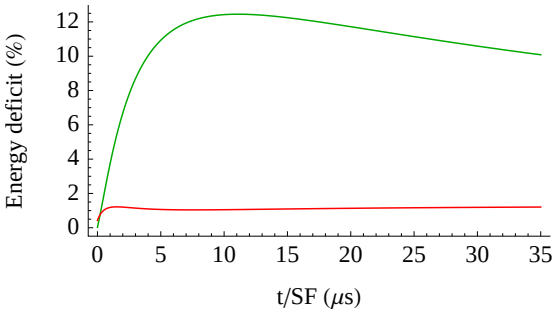

Fig. 10. Wall kinetic energy deficits for the (red) 0.25-scale trace (Fig. 5) and the (green) 0.50-scale trace (Fig. 6) relative to the 2.00-scale trace (Fig. 7).

the kinetic energy difference, $(1 - U_i^2/U_{2.00}^2) \times 100\%$, between the 0.25- and 0.50-scale tests relative to the 2.00 scale case. $U_{2.00}$ is the *fitted* velocity of the 2.0-scale test and U_i is the *fitted* velocity of the 0.25- and 0.50-scale tests. Thus, the fits indicate that the 0.50-scale wall consistently has 99% the energy of the 2.00-scale wall, while the 0.25-scale wall develops 12% less energy than the 2.00-scale wall during the initial 10 μs of motion, but an increasing amount relative to the 2.00-scale wall after 10 μs.

Measured Wall Energy

Cylinder wall energies are typically reported in terms of the kinetic energy of the wall (cylinder specific energy) or the Gurney energy. For a given wall velocity U_i, the cylinder specific energy is simply $E_{KE} = \frac{1}{2}U_i^2$. The Gurney energy varies from this value by a multiplier such that

$$E_G = \left[\frac{1}{2} + \frac{\rho_w}{\rho_e}\left(\frac{R_0^2}{r_0^2} - 1\right)\right]\frac{U_i^2}{2} \tag{6}$$

where ρ_e is the explosive density, ρ_w is the cylinder density, R_0 is the outer wall radius, and r_0 is the inner wall radius.

These measures are computed directly from the experimental wall motion in Fig. 11 and plotted versus the degree of (scaled) cylinder expansion. Researchers traditionally report the wall energy (or

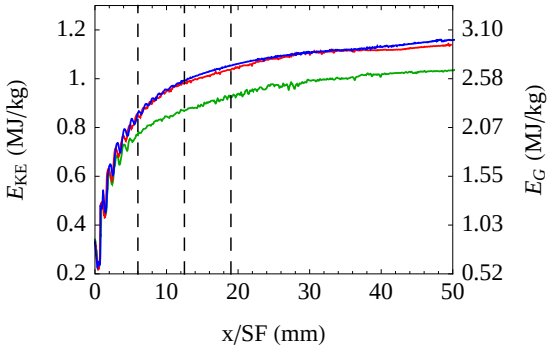

Fig. 11. Energy versus scaled distance. Green = 0.25 scale; red = 0.50 scale, and blue = 2.00 scale.

velocity) at specific scaled distances of 6.0, 12.5, and 19.0 mm as indicated by the dashed lines in Fig. 11. The relative energies reflect the earlier discussion of Fig. 10. Figure 12 shows the integrated wall motion versus time to allow translation between position and time for each trace.

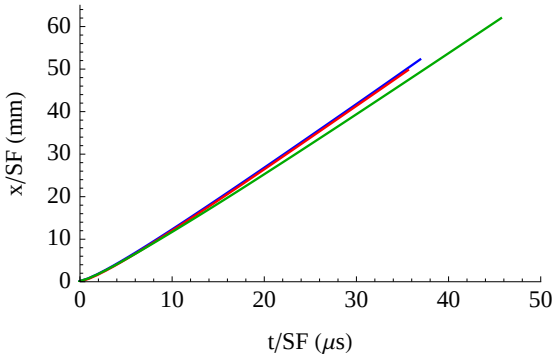

Fig. 12. Scaled position versus time. Green = 0.25 scale; red = 0.50 scale, and blue = 2.00 scale.

Conclusions

Copper cylinder tests were performed at three different scales (0.25, 0.50, and 2.00) relative to the conventional 25.4-mm-inner-diameter test with the insensitive explosive formulation PBX 9502. Detonation velocities, wall motion histories, cylinder kinetic energy histories, and Gurney energies were reported. Analytic functions were fitted to the wall motion to average the effects of wall compressibility and report the data in concise format. The test scale variation allowed evaluation of effect of charge scale on the explosive energy release. It was found that the 0.50-scale experiment released 0.99% of the energy of the 2.00-scale test, while the 0.25-scale experiment only released approximately 88% of the energy of the 2.00-scale test.

References

1. J. Kury, H. Horning, E. Lee, J. McDonnel, D. Ornellas, M. Finger, F. Strange, and M. Wilkins, "Metal acceleration by chemical explosives," in *Fourth Symposium (Int.) on Detonation*, pp. 3–13, Office of Naval Research, 1965.

2. T. Gibbs and A. Popolato, *LASL Explosive Property Data*, pp. 249–258. University of California Press, 1980.

3. R. Catanach, L. Hill, H. Harry, E. Aragon, and D. Murk, "Cylinder test specification," Tech. Rep. LA-13643-MS, LANL, Los Alamos, NM, October 1999.

4. L. Hill, "Detonation product equation of state directly from the cylinder test," in *Proceedings of the 21st International Symposium on Shock Waves*, pp. 355–360, World Scientific Pub Co. Inc., 1997.

5. S. Jackson, "An analytic method for two-dimensional wall motion and product isentrope from the detonation cylinder test," *Proceedings of the Combustion Institute* , 2014. DOI: 10.1016/j.proci.2014.07.071.

6. S. Pemberton, T. Sandoval, T. Herrera, J. Echave, and G. Maskaly, "Test report for equation of state measurements of PBX-9502," Tech. Rep. LA-UR-11-04999, Los Alamos National Laboratory, Los Alamos, NM, 2011.

7. L. Hill and T. Aslam, "Detonation shock dynamics calibration for PBX 9502 with temperature, density, and material lot variations," in *Fourteenth International Detonation Symposium*, pp. 779–788, Office of Naval Research, ONR-351-10-185, 2010.

8. W. Davis, "Cylinder test shot," Tech. Rep. Los Alamos Report M-9-QR-87-3, Los Alamos National Laboratory, Los Alamos, NM, 1987.

9. W. Davis, T. Salyer, S. Jackson, and T. Aslam, "Explosive-driven shock waves in argon," in *13th International Symposium on Detonations*, pp. 1035–1044, Office of Naval Research, 2006.

10. L. Davis and L. Hill, "ANFO cylinder tests," in *AIP Conference Proceedings*, **620**, p. 165, 2002.

11. S. Jackson, C. Kiyanda, and M. Short, "Experimental observations of detonation in ammonium-nitrate-fuel-oil (ANFO) surrounded by a high-sound-speed, shockless, aluminum confiner," *Proceedings of the Combustion Institute* **33**, pp. 2219–2226, 2011.

12. E. Lee, H. Horning, and J. Kury, "Adiabatic expansion of high explosive detonation products," Tech. Rep. UCRL-50422, Lawrence Radiation Laboratory, Livermore, California, 1968.